Astron. Astrophys. 345, 869–883 (1999)

ASTRONOMY AND ASTROPHYSICS

RX J0720.4-3125: Implications for neutron star cooling and the dense matter equation of state

John C.L. Wang[1,⋆], **Bennett Link**[2], **Kenneth Van Riper**[3], **Keith A. Arnaud**[1,4], **and Juan A. Miralles**[5]

[1] Department of Astronomy, University of Maryland, College Park, MD 20742-2421, USA
[2] Department of Physics, Montana State University, Bozeman, MT 59717-0350, USA
[3] White Rock Science, P.O. Box 4729, Los Alamos, NM 87545, USA
[4] Laboratory for High Energy Astrophysics, Goddard Space Flight Center, Greenbelt, MD 20771, USA
[5] Department d'Astronomia i Astrofísica, Universitat de Valéncia, Valencia, Spain

Received 9 October 1998 / Accepted 15 January 1999

Abstract. The soft X-ray source RX J0720.4-3125 appears to be a clean example of a cooling neutron star. Its X-ray emission is well-fit by a 79 ± 4 eV blackbody and displays a periodic modulation with period $P = 8.391$ sec and semi-amplitude $\sim 10\%$. The observational upper limit to the period derivative implies a minimum spindown age of $t_0 = 1.7 \times 10^5$ yr if the star was born rapidly rotating. The absence of a visible supernova remnant independently suggests an age for this source of $\gtrsim 10^5$ yr. With the interpretation of this source as a cooling-driven, magnetized, rotating neutron star, we explore the implications for the dense matter equation of state (EOS), the mode of energy loss (modified URCA vs. direct URCA), and the rate of internal heating due to superfluid friction. For the standard (modified URCA) cooling models, we study two types of stars: those born slowly rotating, with relatively small spin-down rates and conventional dipole magnetic fields ($\sim 10^{12}\,G$), and those born rapidly rotating with large spin-down rates and magnetar-scale dipole fields ($\sim 10^{14}\,G$). We find that standard cooling with a stiff or moderately stiff EOS is consistent with the observations of RX J0720.4-3125 provided the star's age is $\lesssim 3\,t_0 = 5\times10^5$ yr. If the EOS is very stiff, the star must be born with a short rotation period and significant internal heating by superfluid friction is required. More moderate heating suffices only if the star is very massive ($\sim 2\,M_\odot$) and has an age $\sim t_0$. Stars with $M \sim 1.4\,M_\odot$ and a moderately stiff EOS give modulations about a factor of five below that observed. However, the inclusion of atmospheric effects or more complex field geometries could increase the modulation to a level consistent with the observations. Stars with a stiff EOS give modulations close to that observed. As an illustration of the effects of accelerated cooling processes, we consider direct quark URCA cooling. We find that these models cool too fast and are cleanly ruled out for this source. Hence, exotic matter is an insignificant component in the stellar core, or does not participate in accelerated cooling. Direct URCA reactions in nucleonic matter are similarly ruled out. A measure of RX J0720.4-3125's spin-down age would afford crucial tests of our conclusions.

Send offprint requests to: B. Link (blink@dante.physics.montana.edu)
⋆ Deceased

Key words: stars: neutron – stars: evolution – stars: magnetic fields – dense matter – X-rays: stars – stars: individual: RX J0720.4-3125

1. Introduction

The surface thermal emission from the cooling of young neutron stars provides a direct means by which to study the composition of these compact objects and the equation of state of dense matter. There are four pulsars for which thermal X-rays *from cooling* are believed to have been observed with reasonable certainty: PSR B1055-52, B0656+14, Vela and Geminga (Ögelman 1994; Bignami & Caraveo 1996). In each of these cases, nonthermal processes in the magnetosphere and thermal emission from magnetic polar cap heating by particles accelerated in the magnetosphere may also contribute to the total X-ray emission (Halpern & Ruderman 1993; Greiveldinger et al. 1996; Becker & Trümper 1997). The desired thermal component of the emission must be separated from the non-thermal emission in a model-dependent manner (e.g., Finley et al. 1992; Ögelman et al. 1993; Halpern & Ruderman 1993; Ögelman & Finley 1993; Pavlov et al. 1996a; Greiveldinger et al. 1996; Bignami & Caraveo 1996). Ideally, we would like to find neutron stars which show *only* surface thermal emission derived from cooling. In this regard, the two recently discovered soft X-ray sources, RX J185635-3754 (Walter et al. 1996) and RX J0720.4-3125 (Haberl et al. 1997), appear to fit this requirement. The spectra from both sources are best fit with single-component blackbody spectra (57 eV for RX J185635-3754; 79 eV for RX J0720.4-3125), both are steady over timescales ~ 10 yrs, and both are radio and γ-ray quiet. RX J185635-3754 shows no evidence for pulsations at any wavelength (Walter et al. 1996, 1997), and is probably unmagnetized or weakly magnetized. RX J0720.4-3125, however, shows an 8.391 sec periodic modulation in its X-ray light curve and so is most likely moderately to strongly ($\gtrsim 10^{12}\,G$) magnetized. Detailed study of these two sources could offer insights into the character of matter above nuclear density while affording constraints on the physical processes that control the cooling.

The observational upper limit on RX J0720.4-3125's spin-down rate, strengthened by the absence of an associated supernova remnant, indicates that this object is at least 10^5 years old. If this interpretation is correct, RX J0720.4-3125's high temperature of ~ 80 eV poses a serious challenge to neutron star cooling theory. For example, simulations of neutron star cooling indicate an increase in the logarithmic slope of the cooling curve at an age of $\sim 10^4$–10^5 yr as the star makes the transition from neutrino cooling to photon cooling (see Tsuruta 1998 for a comprehensive review). In this paper we study the implications of RX J0720.4-3125 for the dense matter equation of state, the mode of energy loss (modified URCA vs. direct URCA), and possible internal heating from superfluid friction. We conclude that the observations of RX J0720.4-3125 are consistent with a moderately stiff equation of state provided the object's age is in the range $(1\text{–}2)\times 10^5$ yr. A stiff equation of state is viable for a somewhat larger age range $(1\text{–}5)\times 10^5$ yr but requires significant internal heating, through superfluid friction for example, to explain RX J0720.4-3125's high temperature. Accelerated (direct URCA) cooling is inconsistent with the data, even for unrealistically large rates of internal heating, and so is cleanly ruled out by this source.

In Sect. 2, we describe the observations of RX J0720.4-3125. In Sect. 3 we discuss the limits on the age. In Sect. 4, we describe the arguments in favor of an interpretation of RX J0720.4-3125 as a cooling, young neutron star. In Sect. 5, we discuss the modeling of this source. The results and implications are discussed in Sect. 6, and we give our conclusions in Sect. 7.

2. Observations

The source RX J0720.4-3125 is a soft X-ray source with a possible counterpart in the optical band. It was seen by the the EXOSAT LE (Low Energy Detector) and by the ROSAT PSPC (Position Sensitive Proportional Counter) and HRI (High Resolution Imager). The ROSAT PSPC count rate (0.1–2.4 keV) is 1.6 cts s^{-1}, and based upon earlier detections by EXOSAT, is steady ($\lesssim 5\%$ variations) over 12 years (Haberl et al. 1996, 1997). The ROSAT PSPC and HRI light curves both show sinusoidal modulation. A September 1993 PSPC observation yielded a period of 8.3914 ± 0.0002 sec (90% confidence), and a 33 ksec HRI observation in November 1996 gave 8.39115 ± 0.00002 sec (Haberl et al. 1997; hereafter H97). The semi-amplitude modulation, $\mathcal{M} \equiv \frac{C_{max}-C_{min}}{C_{max}+C_{min}}$ (C is the count rate), was $11\pm 2\%$ and $12 \pm 2\%$ for the PSPC and HRI observations, respectively (see Figs. 3 and 6 in H97). The phase-averaged X-ray spectrum is best fit by a single blackbody at $kT = 79\pm 4$ eV with a hydrogen absorption column density of $N_H = (1.3 \pm 0.3)\times 10^{20}$ cm^{-2} (see Table 2 and Fig. 1 in H97). With this spectrum, the unabsorbed source luminosity is

$$L_X \equiv L(0.1-2.4\,\mathrm{keV}) = 8.0\times 10^{31} d_{200}^2 \ \ \mathrm{erg\,s^{-1}}, \qquad (1)$$

where $d = 200 d_{200}$ pc is the distance to the source. In Fig. 1, we show the "on-pulse" spectrum which is defined as the spectrum obtained by averaging over the phases (0.2 – 0.7) that include the maximum of the modulation (see Fig. 3 in H97). For comparison, we also show the "off-pulse" spectrum, obtained by averaging over the remaining phases. The two spectra are indistinguishable; the best-fit parameters are $kT(\mathrm{on}) = 79.7^{+3.7}_{-6.5}$ eV, $N_H(\mathrm{on}) = (1.0^{+0.6}_{-0.3})\times 10^{20}$ cm^{-2} and $kT(\mathrm{off}) = 82.5^{+5.6}_{-5.2}$ eV, $N_H(\mathrm{off}) = (0.8^{+0.5}_{-0.3})\times 10^{20}$ cm^{-2} (errors give 90% confidence range for two parameters of interest).

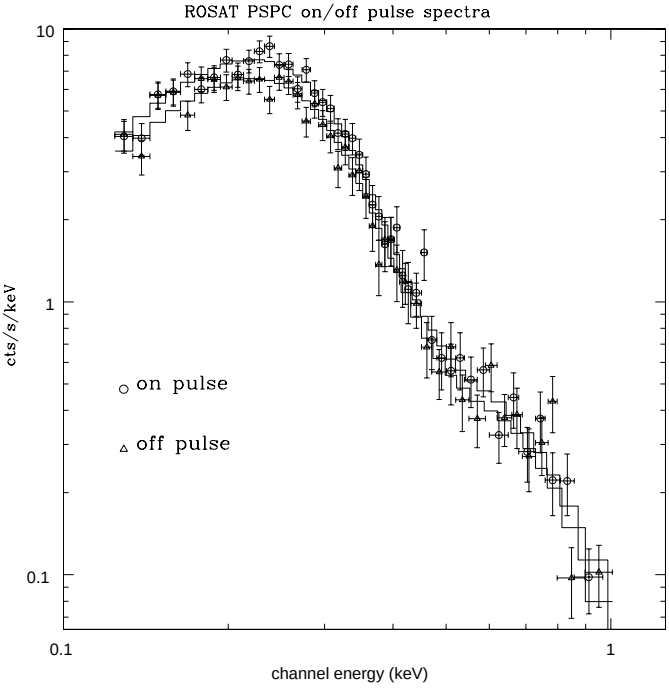

Fig. 1. The on/off pulse spectra of RX J0720.4-3125 obtained from the 3,226 sec ROSAT PSPC observation on 27 September 1993. The on-pulse spectrum (circles) correspond to phases 0.2 to 0.7 in Fig. 3 of H97, while the off-pulse spectrum (triangles) is from phases 0 to 0.2 and 0.7 to 1. The total count rate (0.1–1 keV) in the on (off) pulse spectrum is 1.73 ± 0.04 cts s^{-1} (1.50 ± 0.03 cts s^{-1}). The total count rate (0.1–1) keV in the phase averaged spectrum is 1.61 ± 0.02 cts s^{-1} (cf. H97). Horizontal "error" bars give the energy channel widths. The histograms depict the best single component blackbody fits with $kT(\mathrm{on}) = 79.9$ eV and $kT(\mathrm{off}) = 80.6$ eV ($N_H = 10^{20}$ cm^{-2}).

The 8.391 sec modulation is naturally interpreted as the rotation period of the source (H97; Wang 1997; Konenkov & Popov 1997; Heyl & Hernquist 1998, hereafter HH98). The ROSAT observations are separated by ~ 3 years and show that the pulsed emission is steady. These observations enable H97 to constrain the period derivative to be (90% confidence)

$$-6.0\times 10^{-12} < \dot{P}\,(\mathrm{s\,s^{-1}}) < 0.8\times 10^{-12} \equiv \dot{P}_{max}. \qquad (2)$$

Using $B\,(G) \approx (4\times 10^{39}\,P\,\dot{P})^{1/2}$ from the vacuum dipole model, $\dot{P}_{max}$ gives an upper bound to the surface dipole field strength of $\sim 10^{14}\,G$. With such fields and a period of 8.391 sec, one cannot rule out the possibility that this source is a radio pulsar since it could easily lie above the empirical, extrapolated, radio pulsar death line ($B = 0.2P^2$; Chanmugam 1992). However, a radio pulsar with an 8.391 sec period would have a very narrow (radio) beaming cone and hence could easily go unde-

tected (e.g., Narayan & Vivekanand 1983; Lyne & Manchester 1988; Emmering & Chevalier 1989).

Two pointed ROSAT HRI observations (Haberl et al. 1996, 1997) secured the position of the source to be (J2000) $\alpha = 7$h, 20m, 24.90s; δ =-31° 25′ 51.3″ (with $\pm 3''$ uncertainty). The corresponding Galactic coordinates are $l = 244°$, $b = -8.1°$. Deep optical observations by the ESO-NTT reveal two possible counterparts, stars X1 and X2, with $B = 26.1 \pm 0.25$ and $B = 26.5 \pm 0.30$, respectively (Motch & Haberl 1998), while observations by Keck II reveal a possible counterpart in the X-ray error box, designated star X, with $B = 26.6 \pm 0.2$ and $R = 26.9 \pm 0.3$ (Kulkarni & van Kerkwijk 1998). The star X of Kulkarni & van Kerkwijk (1998) is the same as star X1 of Motch & Haberl (1998). From its location and blue color, Kulkarni & van Kerkwijk argue that star X (=star X1) is the more likely counterpart to RX J0720.4-3125. The absence of an optical counterpart brighter than $B = 26.1$ sets a lower bound on the X-ray to optical flux ratio f_X/f_V of $\sim 10^5$ (assuming $f_V \sim f_B$; Kulkarni & van Kerkwijk 1998). Such a huge ratio rules out all known astronomical sources except for an isolated neutron star (see, e.g., Stocke et al. 1991, 1995).

The observational evidence strongly suggests that RX J0720.4-3125 is a slowly rotating, magnetized, isolated, neutron star. We adopt this interpretation in the following.

3. The age of RX J0720.4-3125

Assuming that it was born with a period $P_i \ll P$, the spindown age of RX J0720.4-3125, assuming a braking index of 3, is

$$t_S \equiv \frac{P}{2\dot{P}}. \tag{3}$$

From its period and $\dot{P}_{max}$ (Eq. (2)), we get a lower limit to the source's spindown age of

$$t_0 = 1.7 \times 10^5 \text{ yr}. \tag{4}$$

The absence of any obvious supernova remnants in the general direction of this source (Green 1996) also suggests that this source cannot be much younger than $\sim 10^5$ yrs; otherwise the remnant should be visible in optical and/or X-rays (e.g., McCray 1987). It is possible, however, that this source has a very large transverse velocity so that it has migrated far from its original line of sight. With a transverse velocity $v_t = 300 v_{t,300}$ km s^{-1}, a distance $d = 200 d_{200}$ pc, and travel time $t = 10^5 t_5$ yrs, this source could have originated $\sim 9° \, v_{t,300} t_5 / d_{200}$ from its present line of sight. The only obvious structure in this vicinity is an evacuated "tunnel" which appears to be a part of the Local Bubble (Welsh et al. 1994). Indeed, the line of sight to this source is only about 15° from the center of this tunnel (at $l \sim 230°$; see Fig. 3 in Welsh et al. 1994). It is intriguing to speculate that RX J0720.4-3125 may be the result of a supernova that occurred $\lesssim 10^6$ yrs ago and which created the Local Bubble (e.g., Edgar 1986; Cox & Anderson 1982). The feasibility of this idea must await proper motion and distance (parallax) measurements.

Once $\dot{P}$ has been measured, the source's age can be determined, inasmuch as the spindown age is an accurate measure of the star's true age. If the star was born slowly rotating (e.g., Spruit & Phinney 1998), the age will also depend upon the (unknown) birth period (cf. Eq. (11); Sect. (6.2)) and can take any value. For example, with a small $\dot{P}$ and a P_i which is not near the present day period P, the star's age can be $\gg t_0$. Alternatively, the star's age can be $\ll t_0$ if the birth period P_i is very near P. The absence of any obvious supernova remnant near the source, however, argues against an age much younger than $\sim 10^5$ yr, consistent with the lower bound on the age t_0 obtained assuming a rapid spin rate at birth.

4. Origin of the X-rays

There are three possibilities for the origin of the X-rays from this source: rotation, accretion, and cooling. We discuss each in turn in this section and argue for the cooling interpretation.

There is no compact nonthermal X-ray nebula associated with this source (cf. Vela; Ögelman et al. 1993) and the (phase-averaged) spectrum of this source is extremely well-fit by a single component blackbody (H97). Thus, if RX J0720.4-3125 is a rotation-powered pulsar, any contributions to the X-rays from nonthermal (e.g., magnetospheric) processes associated with the radio/γ-ray pulsar mechanism are negligible. [1] In sources where the X-rays are driven by the spindown power, typically $L_X/\dot{E} \sim 10^{-3}$ (Becker & Trümper 1997), whereas for this source, using the spindown power $\dot{E} = I\Omega\dot{\Omega}$, Eq. (1) and $\dot{P}_{max}$ from Eq. (2) gives

$$\frac{L_X}{\dot{E}} \gtrsim 2 \, d_{200}^2 \, I_{45}^{-1}, \tag{5}$$

where $I = 10^{45} I_{45}$ g cm^2 is the star's moment of inertia. The (thermal) contribution from polar cap heating associated with magnetospheric particle acceleration must therefore also be negligible. We conclude that the bulk of the X-rays must have a non-rotationally-driven origin.

Another possibility for the origin of the X-rays is accretion from the interstellar medium (H97; Konenkov & Popov 1997; Wang 1997). Recent observational and theoretical work, however, now cast doubt on this interpretation. If the source is accreting from the ISM, the rate required to produce the observed X-ray flux is $\dot{M} \sim 10^{11}$ g s^{-1}, assuming Bondi-Hoyle accretion (H97; Konenkov & Popov 1997; Wang 1997). At this rate, it would take only $\sim 10^2$ sec for the star to acquire a hydrogen-rich atmospheric layer with column depth ~ 1 g cm^{-2} (corresponding to a photospheric density of ~ 1 g cm^{-3} [e.g., Joss & Rappaport 1984] and scale height of ~ 1 cm for a H-rich atmosphere at $\sim 10^6$ K; see also Zavlin et al. 1996). The atmosphere must then be only weakly magnetized because for accretion to be occurring now, the stellar field must satisfy $B \lesssim 10^{10}$ G to overcome the propeller effect (H97; Konenkov & Popov 1997;

[1] A nonthermal component may be responsible for the *optical* excess observed in B and R (a factor of ~ 5 above the Rayleigh-Jeans extrapolation of a 79 eV blackbody; Kulkarni & van Kerkwijk 1998; Motch & Haberl 1998), though this excess could also have other causes such as the composition of the neutron star atmosphere (e.g., Pavlov et al. 1996b; Shibanov et al. 1992).

Table 1. Neutrino emission processes

Process		Emissivity[a,c] ($\mathrm{erg\,cm^{-3}\,s^{-1}}$)	Reference
Modified URCA[b]	$\begin{cases} n+N \to N+p+e+\overline{\nu}_e \\ e+p+N \to N+n+\nu_e \end{cases}$	$\sim 10^{20}\,T_9^8$	Friman & Maxwell 1979
Core bremsstrahlung	$\begin{cases} n+n' \to n+n'+\overline{\nu}_e+\nu_e \\ n+p \to n+p+\overline{\nu}_e+\nu_e \\ e+p \to e+p+\overline{\nu}_e+\nu_e \end{cases}$	$\sim 10^{19}\,T_9^8$	$\begin{cases}\text{Friman \& Maxwell 1979,} \\ \text{Maxwell 1979}\end{cases}$
Crust bremsstrahlung	$e+(A,Z) \to e+(A,Z)+\overline{\nu}_e+\nu_e$	$\sim 10^{20}\,T_9^6$	Itoh et al. 1984
Quark URCA	$\begin{cases} d \to u+e+\overline{\nu}_e \\ u+e \to d+\nu_e \end{cases}$	$\sim 10^{26}\,\alpha_c\,T_9^6$	Iwamoto 1980

[a] T_9 is temperature in units of $10^9\,K$.
[b] N is a spectator nucleon to ensure energy-momentum conservation
[c] α_c is the strong interaction (QCD) coupling constant.

Wang 1997). For a given X-ray (photon) flux, such an atmosphere should appear very bright in the optical (Pavlov et al. 1996b; Zavlin et al. 1996; Rajagopal & Romani 1996). For a fixed X-ray flux, the ratio of the optical flux from an atmosphere with an effective temperature T_{atm} to that from a blackbody at temperature T_{BB} is

$$\frac{F_{opt}^{atm}}{F_{opt}^{BB}} \approx \beta \left(\frac{T_{BB}}{T_{atm}}\right)^2 \left(\frac{f_{BB,X}}{f_{atm,X}}\right), \qquad (6)$$

where the f factors give the fraction of the photon flux emitted in X-rays (between 0.1 and 2.4 keV), and the optical flux for the atmosphere is given by the Rayleigh-Jeans relation $F_{opt}^{atm} \propto \beta\, T_{atm}$ with $\beta \leq 1$ (Zavlin et al. 1996). For a weakly magnetized ($B < 10^{10}\,G$) hydrogen-rich atmosphere, $T_{atm} = 27$ eV for $T_{BB} = 79$ eV (Rajagopal & Romani 1996; Motch & Haberl 1998), $\beta \approx 0.33$ (Zavlin et al. 1996), and $F_{opt}^{atm}/F_{opt}^{BB} \approx 10$. Recent observations, however, give $F_{opt}^{obs}/F_{opt}^{BB} \lesssim 5$ (Motch & Haberl 1998; Kulkarni & van Kerkwijk 1998; see also footnote 2). A weakly magnetized hydrogen-rich atmosphere thus seems unlikely, although it cannot yet be ruled out with certainty. On the other hand, the observations are consistent with an iron-rich atmosphere, which displays a broad band spectrum more closely resembling a blackbody at the same effective temperature as the iron atmosphere (e.g., Pavlov et al. 1996b; Rajagopal et al. 1997). Such an atmosphere would be consistent with a young neutron star that has never experienced accretion, either from fall-back material in the supernova debris or from its surroundings. [2] In this respect, this source is similar to RX J185635-3754 (Pavlov et al. 1996b; Walter et al. 1997).

On the theoretical side, Wang & Sutherland (1998) have shown that ISM accretion at the level of $\sim 10^{11}\,\mathrm{g\,s^{-1}}$ is most likely highly time-dependent with variability on timescales $\sim$ months to years. This is due primarily to photoionization heating of infalling gas which creates an enormous overpressure in the accretion region (at $r \lesssim GM/a_\infty^2$, a_∞ = sound speed in ambient medium) relative to ambient interstellar gas. [3] The X-ray observations show, however, that this source is very steady over timescales of $\sim$ 10 years. This is more suggestive of passive cooling than a dynamical accretion process at work.

5. Modeling the cooling

5.1. Cooling processes

We use the 1-D code of Van Riper (1991) including magnetic fields and internal frictional heating (Van Riper et al. 1995; hereafter VLE) to treat the thermal evolution. The neutrino production processes are listed in Table 1; these include the modified URCA reactions for standard cooling models (Friman & Maxwell 1979), core bremsstrahlung (Friman & Maxwell 1979; Maxwell 1979), and crust bremsstrahlung (Itoh et al. 1984). [4] It is possible that quarks, pions, kaons or hyperons appear at high densities (see, e.g., Brown et al. 1988; Pandharipande 1971; Glendenning 1985). Direct URCA processes associated with these degrees of freedom would give greatly accelerated cooling. The direct URCA process would also occur in non-exotic matter if the proton fraction exceeds $\sim$ 11% (see, e.g., Lattimer et al. 1991). To treat these possibilities, we consider the direct URCA process on non-superfluid quarks (Iwamoto 1980) as an example of an accelerated cooling process. We have not included modification of the neutrino emissivity by medium effects (Voskresensky & Senatorov 1986) or the contribution of superfluid pair breaking and formation (Voskresensky & Senatorov 1987). Because these effects enhance the neutrino emissivity relative to the modified URCA rate, the standard and accelerated cooling models considered here are adequate to bracket the

[2] A strongly magnetized hydrogen-rich atmosphere is also allowed by the observations. Such an atmosphere may arise if shortly after the supernova event a young star accreted fall-back material from the supernova debris. Owing to the strong field, the star will not be able to accrete from the interstellar medium.

[3] Their calculations were carried out in the limit of spherical accretion (1-D). The inferred velocity of RX J0720.4-3125, were it undergoing Bondi-Hoyle accretion, is $< 20\,\mathrm{km\,s^{-1}}$, and so applying the 1-D approximation to this source should be adequate (Wang 1997).

[4] We have not included the proton branch in the core bremsstrahlung ($p+p' \to p+p'+\overline{\nu}_e+\nu_e$; Yakovlev & Levenfish 1995).

range of possible cooling behavior. We will return to a discussion of medium effects and superfluid pair breaking in Sect. 7.

We consider neutron and proton superfluidity using the neutron gap calculations of Takatsuka (1972) and the proton gap calculations of Chao et al. (1972). Superfluidity suppresses the core neutrino production reactions involving nucleons and reduces the nucleon contribution to the specific heat. The effect of superfluidity is particularly important for a star with a stiff equation of state where neutrons and protons are superfluid throughout the stellar core – these stars cool much more rapidly after $\sim 10^4$–10^5 yr than if there were no superfluidity (Van Riper 1991). Proper treatment of this effect is particularly important for the modeling of RX J0720.4-3125 (cf. Sect. 6). In the outer crust (the *envelope*, where $\rho \leq 10^{10}\,\mathrm{g\,cm^{-3}}$), we use magnetic conductivities from Hernquist (1985) which are valid for $B \leq 10^{14}\,G$. Magnetic fields affect the cooling by enhancing heat transport (mainly by electron thermal conduction) along field lines while suppressing transport across field lines. In stars with very strong dipole fields ($B \gtrsim 10^{13}\,G$), the former effect dominates over the latter, while the latter effect dominates when $B \lesssim 10^{12}\,G$ (Shibanov & Yakovlev 1996). Our code can treat geometries where the magnetic field is everywhere radial (monopolar geometry) and where it is everywhere parallel to the stellar surface (tangential geometry). The composition of the envelope and atmosphere is taken to be iron and the atmosphere is assumed to radiate as a blackbody.

5.2. Heating processes

Differential rotation between the neutron star crust and the neutron superfluid it is expected to contain could generate significant heat through friction, increasing the star's temperature and enhancing its thermal emission. The total rate of heat generation is (Shibazaki & Lamb 1989; VLE; Umeda et al. 1993)

$$H(t) = \Delta J_s \left|\dot{\Omega}\right| \equiv I_s \bar{\omega} \left|\dot{\Omega}\right| \tag{7}$$

where ΔJ_s is the excess angular momentum residing in the superfluid, I_s is the moment of inertia of the portion of the superfluid that is differentially rotating, and $\bar{\omega}$ is the angular velocity difference between the two components averaged over the superfluid moment of inertia. In principle, the heat could be generated anywhere in the star in which there are superfluid neutrons. Usually, however, the superfluid in the core is regarded as tightly coupled to the rotation of the solid through Fermi liquid effects (Alpar et al. 1984). Analyses of glitch data (Abney et al. 1996) and spin variations in accreting neutron stars (Boynton et al. 1984) and in isolated pulsars (Boynton 1981; Deeter 1981) support this picture. In the inner crust, however, interaction between crustal nuclei and superfluid vorticity can lead to substantial differential rotation (see, e.g., Anderson & Itoh 1975) and heating. The velocity difference that can develop is determined by uncertain microphysics, however, $\bar{\omega}$ could plausibly be as large as 100 rad s^{-1} (Epstein & Baym 1988). In a star with a stiff equation of state and a thick crust, ΔJ_s could then be as large as $\sim 6\times10^{46}$ g cm^2 rad s^{-1}. The rate of heat generation is then of the order

$$H(t) = \left(\frac{\Delta J_s}{6\times10^{46}\ \mathrm{g\ cm^2\ s^{-1}}}\right)\left(\frac{P}{8.4\ \mathrm{s}}\right)^{-1} \times \left(\frac{t_S}{1.7\times10^5\ \mathrm{yr}}\right)^{-1} L_\odot, \tag{8}$$

where P is the star's spin period, t_S is the spindown age (Eq. (3)), and a rapid initial spin rate was assumed. A heating rate this large is most important in a star's thermal evolution after $\sim 10^5$ yr, when $H(t)$ becomes comparable to the luminosity from residual heat. However, given the uncertainties in the microphysics of the superfluid's interaction with the normal matter (e.g., Epstein & Baym 1988; Alpar et al. 1989; Umeda et al. 1993; VLE), we will treat ΔJ_s as a free parameter, and regard $\bar{\omega} = 100$ rad s^{-1} as an upper limit.

Another process that heats the star is structural relaxation occurring as the star spins down and becomes less oblate. If structural relaxation occurs violently as starquakes, for example, the rate of heat generation is (Cheng et al. 1992),

$$H_{\mathrm{quake}} \sim \frac{\mu\theta_{\max}^2}{t_{\mathrm{S}}} = 6\times10^{-5}\left(\frac{\mu}{10^{48}\ \mathrm{erg}}\right)\left(\frac{\theta_{\max}}{10^{-3}}\right)^2 \times \left(\frac{t_{\mathrm{age}}}{1.7\times10^5\ \mathrm{yr}}\right)^{-1} L_\odot, \tag{9}$$

where μ is the shear modulus of the crust and $\theta_{\max}$ is the critical strain angle at which the crust breaks. This heating rate is far smaller than the rate due to superfluid friction estimated in Eq. (8), and so will be neglected in this study.

Other possible heat sources include departures from β-equilibrium as the star spins down (Reisenegger 1995) and decay of a magnetar-scale field (Thompson & Duncan 1996; Heyl & Kulkarni 1998). The former effect is probably unimportant for fields $\gg 10^{10}\,G$ and so we do not consider it in this paper. While decay of a superstrong field is a possible heat source for RX J0720.4-3125, it is not required by the existing data (see Sect. 6). We focus here on a critical examination of thermal evolution using a centered dipole geometry for the surface magnetic field. More complicated field geometries (e.g., quadrupolar) have very little effect on the cooling behavior (e.g., Page & Sarmiento 1996).

5.3. Spindown model

A spindown relationship is needed in order to obtain the star's period and period derivative as functions of the age. For illustration, we take the vacuum dipole model with a braking index of three in all our calculations. We have also considered models with braking indices other than three and find the effect on the star's thermal evolution to be small. Thus, for $\dot{\Omega}$, we use the spindown law

$$\dot{\Omega} = -K\,\Omega^3, \tag{10}$$

where K is a parameter which can be determined from the star's spindown age t_S (Eq. (3)). The star's age inferred from Eq. (10) is

$$t_{spin} = t_S \left[1 - \left(\frac{P_i}{P}\right)^2\right], \tag{11}$$

where the spindown age is

$$t_S \equiv \frac{P}{2\dot{P}} = \frac{1}{2\,K}\left(\frac{P}{2\pi}\right)^2. \tag{12}$$

In this spindown model, the spindown age t_S is the star's actual age if it was born spinning rapidly, that is, $t_S = t_{spin}(P_i \ll P)$ (cf. Eq. (11)). We obtain K from Eq. (12) given t_S and P (or equivalently, P and $\dot{P}$; see Sect. 5.5). Alternatively, K can be treated as a free parameter.

In the vacuum dipole model of pulsar spin down, the relation between K and B is

$$K = \frac{B^2\,R^6}{6\,I\,c^3}, \tag{13}$$

where R is the radius of the star, I is its moment of inertia, and c is the speed of light. [5] Stars with low B have smaller K, spin down slower (Eq. (10)) and have long spindown ages t_S (Eq. (12)). However, the "actual" age is given by t_{spin} (Eq. (11)) and can be much less than t_S if the birth period P_i is close to the present day period P. By contrast, stars with high B spin down quickly and have short t_S and t_{spin}. Stars which are born slowly rotating must have conventional fields ($\lesssim 10^{13}\,G$) to ensure that they do not spin down too quickly (Eq. (11)), while those born rapidly rotating must have magnetar scale fields ($\sim 10^{14}\,G$; Duncan & Thompson 1992) to spin them down to $P = 8.391$ sec in $\sim 10^5$ yr (Sect. 3).

While the existence of radio pulsars shows that many neutron stars are born rapidly rotating, there is no compelling reason to believe that all neutron stars are born this way. For instance, based on radio pulsar population synthesis calculations, Chevalier & Emmering (1986) and Emmering & Chevalier (1989) argue that most pulsars are born with periods > 0.5 sec (see also Narayan & Ostriker 1990; Lamb 1992). These authors assumed exponential field decay over $\sim 10^7$ yr, whereas the current thinking is that fields on isolated neutron stars decay only very slowly or not at all (Bhattacharya et al. 1992; Lamb 1992; Wakatsuki et al. 1992; Goldreich & Reisenegger 1992; Verbunt 1994; Kulkarni & Anderson 1996). However, more recently, by studying the kick(s) that neutron stars may receive at birth, Spruit & Phinney (1998) argue that many neutron stars are born slowly rotating with birth periods > 2 sec and they speculate that RX J0720.4-3125 might belong to this group of slow rotators.

5.4. Surface temperature distribution and the observed flux

The thermal conductivity in a magnetized neutron star depends on the angle between the heat current and the magnetic field. The anisotropic conductivity in the crust creates a distribution of the temperature over the stellar surface. Shibanov & Yakovlev (1996; see also Greenstein & Hartke 1983; Page 1995) have proposed an approximate solution to the thermal diffusion equation that accounts for this effect and which requires only a 1-D computer code. In this prescription, for a given model, we compute two cooling histories, one with a radial (monopolar) field geometry and one with a tangential field geometry (where the field is everywhere perpendicular to the radial direction). The surface temperature distribution is given by

$$T_s^4(B,t,\Theta) = T_\parallel^4(B,t)\,\cos^2\chi + T_\perp^4(B,t)\,\sin^2\chi, \tag{14}$$

where $T_\parallel$ ($T_\perp$) is the temperature obtained from the cooling history using a radial (tangential) field geometry. The angle Θ is the magnetic colatitude and χ is the angle between the magnetic field and the local surface normal. The magnetic colatitude measures the angle between the star's magnetic moment and any point on the stellar surface. The relation between χ and Θ depends upon the surface field geometry (see, e.g., Eq. (15)). The derivation of Eq. (14) is based on the assumption that, at any given point on the star, the heat flux through the subphotospheric layers is predominantly in the radial direction, which, owing to the large conductivity along the field compared to that across the field (i.e., $\kappa_\parallel \gg \kappa_\perp$), is generally a very good approximation (Greenstein & Hartke 1983; Shibanov & Yakovlev 1996). The use of Eq. (14) to describe the temperature across the entire stellar surface is valid if the inner crust is nearly isothermal. In the absence of heating, we find that the stellar core and inner crust become nearly isothermal (temperature independent of radius in the 1-D runs) after $\ll 10^4$ yr, which is much shorter than the $\gtrsim 10^5$ yr timescales of interest to us. When internal frictional heating is included, the heat production is not uniform and occurs primarily around the rotational equator near the inner crust-core boundary at depths ~ 0.1–1 km (depending on EOS) where $\rho \sim 10^{14}\,\mathrm{g\,cm^{-3}}$ (VLE). However, under fairly general conditions, owing to the high electron conductivities in the inner crust compared to that in the outer crust (where $\rho \sim 10^6\,\mathrm{g\,cm^{-3}}$), the deposited heat will very quickly spread around the inner crust rendering it isothermal. Hence, the angular dependence of the heating rate, neglected here, will have a small effect on the surface temperature distribution, and Eq. (14) can still be used in the presence of heating. Our results are insensitive to the density at which the heat is deposited for densities $\gtrsim 10^{13}\,\mathrm{g\,cm^{-3}}$; in our simulations, we deposit most of the heat at $10^{14}\,\mathrm{g\,cm^{-3}}$. In all of our calculations, we compute the full thermal evolution, that is, we do not use the isothermal approximation. A realistic $T_s(\Theta)$ requires a full 2-D calculation where tangential heat flow between different Θ is properly accounted for. Such calculations are being done, and should bear fruit in the near future (see, e.g., Schaaf 1990; Tsuruta 1998; Tsuruta 1998, private communication; see also Schaab & Weigel 1998 for most recent work). Tangential heat flow will likely reduce the temperature contrast between pole and equator and so Eq. (14) probably gives an upper bound to the temperature contrasts expected on a real star (Shibanov & Yakovlev 1996). In general,

[5] Using Eqs. (13) and (12), $R = 10\,\mathrm{km}$, and $I = 10^{45}\,\mathrm{g\,cm^2}$ gives $B = (4\times 10^{39}\,P\,\dot{P})^{1/2}\,G$.

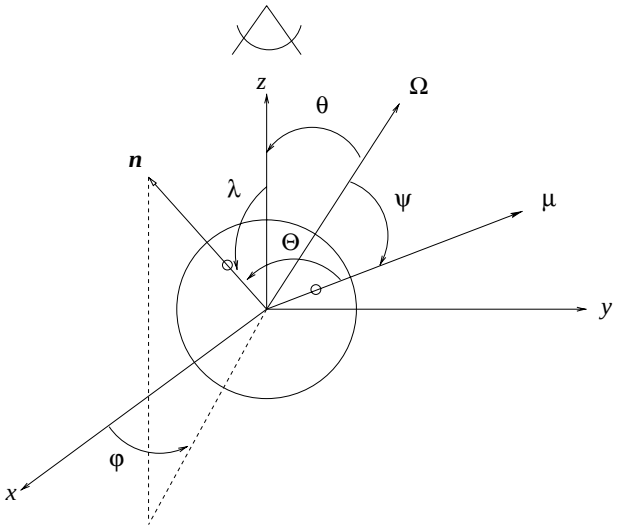

Fig. 2. The geometrical setup used to calculate the photon flux at the observer (Eq. (16)). The line of sight to the observer is along the z axis ($\parallel \mathbf{n}_{los}$). The angle between the rotation axis $\mathbf{\Omega}$ and line of sight is θ, and that between the rotation axis and magnetic dipole moment $\boldsymbol{\mu}$ is ψ. The location in the xyz coordinate system of an emitting patch is given by (λ, φ) with $\mathbf{n}$ the normal to this patch. The magnetic colatitude Θ gives the angle between $\boldsymbol{\mu}$ and $\mathbf{n}$. The rotation phase Φ (not shown) is measured about the rotation axis $\mathbf{\Omega}$, with $\Phi = 0, \pi$ when $\mathbf{\Omega}$, $\boldsymbol{\mu}$, and $\mathbf{n}_{los}$ are coplanar.

however, Eq. (14) should be a reasonable first approximation to the anisotropic surface temperature distribution.

For a centered dipole field,

$$\tan\chi = \frac{1}{2}\tan\Theta. \tag{15}$$

We ignore general relativistic effects on the dipole field geometry. Although general relativistic effects make the field more radial (Ginzburg & Ozernoy 1964), the effect on the cooling is negligible for $B < 10^{14}\,G$ (Shibanov & Yakovlev 1996).

To relate the emitted flux from the stellar surface to the observed flux, we use the geometrical setup shown in Fig. 2. We define the line of sight to be directed along the coordinate z axis and to lie in the same (y-z) plane as the rotation axis. The angle between the rotation axis, $\mathbf{\Omega}$, and line of sight, $\mathbf{n}_{los}$, is θ, and ψ is the angle between the rotation axis and magnetic dipole axis, $\boldsymbol{\mu}$ (an orthogonal rotator has $\psi = \pi/2$). The location of an arbitrary area element (with local surface normal $\mathbf{n}$) on the spherical stellar surface is specified by the angles λ and φ. The surface temperature distribution as viewed by a distant observer is given by $T_s^\infty(\lambda,\varphi)$. Following Page (1995), including general relativistic light bending, the incident, phase-dependent, absorbed (by the ISM), photon flux (in photons cm^{-2} s^{-1} keV^{-1}) at the observer is given by

$$\frac{d\mathcal{N}}{dA_\infty\, dt_\infty\, dE_\infty} = \frac{2}{h^3c^2}\,\frac{R_\infty^2}{D^2}\,\mathrm{e}^{-\sigma(E_\infty)\,N_H} \times \int_0^{2\pi} d\varphi \int_0^{\pi/2} \sin\delta\,\cos\delta\, d\delta\, \frac{E_\infty^2}{\exp[\frac{E_\infty}{kT_s^\infty(\lambda,\varphi)}]-1}, \tag{16}$$

where D is the distance to the source, R_∞ and E_∞ are the stellar radius and photon energy as measured by a distant observer, $\sigma(E_\infty)$ is the photoelectric absorption cross section (in cm^2 per hydrogen atom; Morrison & McCammon 1983), N_H is the hydrogen column density to the source, M is the gravitational mass of the star, and R is the star's intrinsic radius. The effect of general relativistic light bending is included with the $\sin\delta\cos\delta\, d\delta$ factor in Eq. (16). The angle δ is the angle between the local surface normal of an emitting patch located at angle λ (see Fig. 2) and the emergent light ray which makes its way to the observer (see Fig. 2 in Page 1995). The relation between δ and λ is given by (Page 1995)

$$\lambda = \lambda(\sin\delta) = \int_0^{GM/Rc^2} \frac{\sin\delta\, du}{\left[\left(1-\frac{2GM}{Rc^2}\right)\left(\frac{GM}{Rc^2}\right)^2 - (1-2u)\,u^2\,\sin^2\delta\right]^{1/2}}. \tag{17}$$

In the flat space (Newtonian) limit, $GM/Rc^2 \to 0$, so that $\delta = \lambda$ and $\sin\delta\cos\delta\, d\delta \to \sin\lambda\cos\lambda\, d\lambda$. For finite GM/Rc^2, however, $\lambda_{max} = \lambda(1) > \pi/2$ and more than half the star becomes visible. As a result, the star appears larger than R, with

$$R_\infty = \frac{R}{\left[1-\frac{2GM}{Rc^2}\right]^{1/2}} > R \tag{18}$$

(cf. Shapiro & Teukolsky 1983; Page 1995). We have assumed that the surface emits locally everywhere as a blackbody. That is, the specific intensity (in ph cm^{-2} s^{-1} keV^{-1} str^{-1}) at any point on the surface is given by $I_E = [2/(h^3c^2)]\,E_\infty^2/(\mathrm{e}^{E_\infty/kT_s^\infty}-1)$. As discussed in Sect. 4, this is a reasonable assumption to adopt for iron atmospheres. In our models, $T_s^\infty = T_s^\infty(\Theta)$ is given by Eqs. (14) and (15). The magnetic colatitude Θ ($\Theta = 0, \pi$ at the magnetic poles and $\Theta = \pi/2$ at the magnetic equator) is given by

$$\begin{aligned}\cos\Theta = \frac{\boldsymbol{\mu}\cdot\mathbf{n}}{|\boldsymbol{\mu}|} &= \sin\psi\,\sin\Phi\,\sin\lambda\,\cos\varphi \\ &- \sin\psi\,\cos\theta\,\cos\Phi\,\sin\lambda\,\sin\varphi - \cos\psi\,\sin\theta\,\sin\lambda\,\sin\varphi \\ &+ \cos\psi\,\cos\theta\,\cos\lambda - \sin\psi\,\sin\theta\,\cos\Phi\,\cos\lambda,\end{aligned} \tag{19}$$

where Φ is the rotational phase with $\Phi = 0, \pi$ defined to be when $\mathbf{n}_{los}$, $\mathbf{\Omega}$, and $\boldsymbol{\mu}$ are coplanar.

5.5. Simulations and comparison with observations

The parameters and physical processes of our models that control the thermal evolution are: the stellar mass M, dense matter equation of state (EOS), cooling mechanism (standard vs accelerated cooling), heating rate and magnetic field strength B. The heating rate $H(t)$ depends on $\dot{\Omega}$ (Eq. 7), and hence depends on the star's birth period P_i, age, and braking index n (fixed at three).

We consider three representative equations of state whose characteristics are expected to bracket those of the actual dense matter equation of state: BPS (soft; Baym et al. 1971), PS (stiff; Pandharipande & Smith 1975), and FP (intermediate; Friedman & Pandharipande 1981). For the neutron and superfluid gaps adopted here, BPS and FP stars have high enough core densities that the matter is normal there; PS stars are superfluid

Table 2. Neutron star attributes

Mass $M_\odot$	EOS	R (km)	ρ_c (g cm^{-3})	I (g cm^2)
1.4	BPS	7.34	4.89×10^{15}	6.5×10^{44}
1.4	FP	10.57	1.27×10^{15}	1.1×10^{45}
1.4	PS	15.83	4.69×10^{14}	2.2×10^{45}
1.0	FP	11.21	9.14×10^{14}	7.75×10^{44}
1.0	PS	16.44	3.31×10^{14}	1.49×10^{45}
1.97	FP	9.25	2.97×10^{15}	1.63×10^{45}
1.96	PS	13.67	1.55×10^{15}	2.57×10^{45}

throughout. The attributes of the stars in our study are listed in Table 2. Most of the models we consider are for a mass of 1.4 $M_\odot$ (all masses are gravitational masses), since actual neutron star masses appear to follow a narrow distribution about this value (Thorsett & Chakrabarty 1998; Nagase 1989).

We divide our models into two groups - stars born slowly rotating (S stars; $P \simeq P_i$) and stars born rapidly rotating (R stars; $P_i \ll P$). A summary of the parameters we used for our models is displayed in Table 3.

The S stars have small $\dot{\Omega}$ and hence weaker fields ($\lesssim 10^{13}\,G$) than the R stars; we take $B = 10^{12}\,G$ as a representative field for these stars. Since we do not specify P_i, the star can be of any age (but not much less than $\sim 10^5$ yr; Sect. 3). Since the spin-down rate is small for S stars we neglect heating, thus removing any dependence of the thermal evolution on K and P_i.

The R stars must have a strong field to be spun down to 8.391 sec before the star gets too cold at several hundred thousand years. The corresponding large spin-down rates could drive significant heating from superfluid friction (Eq. (7)). Using Eqs. (11), (12) and (13) with $R \sim 10$ km and $I \sim 10^{45}$ g cm^2 suggests that fields $\sim 10^{14}\,G$ are required, and we take $B = 10^{14}\,G$ as the representative field (Sect. 5.3). After at most a few thousand years, the thermal evolution of these models becomes independent of P_i, and the age equals the spindown age t_S (Eq. (12)). We consider heating for R stars with the FP and PS equations of state; BPS stars have little superfluid content and internal friction has only a small effect on the thermal evolution (Van Riper 1991; VLE). We consider two levels of heating: $\bar{\omega} = 10$ and 100 rad s^{-1} (Eq. 7).

We constrain the cooling models in the following way. For S stars, the phase-averaged spectrum must be well-fit by a single-component blackbody at $T_{eff} = 79 \pm 4$ eV at an age $\gtrsim 10^5$ yr (Sects. 2, 3). For R stars without heating, we require this T_{eff} at an age $\gtrsim t_0$ (Eq. (4); Sect. 3). For R stars with heating, a spindown age $t_S \gtrsim t_0$ (Eq. (12)) must be assumed (Table 3), and we require T_{eff} at the assumed age.

At each stage in a model's evolution, we determine T_{eff} as follows. First, we find the cooling curves $T_\parallel(t)$ and $T_\perp(t)$ for radial and tangential field geometries, respectively. We then construct the 2-D surface temperature distribution from Eqs. (14) and (15) using as representative geometrical parameters $\theta = \psi = 30^\circ$. (Fixing θ and ψ is justified because the variation in T_{eff} is $< 5\%$ over the whole range of θ and ψ.) We choose θ and ψ to be less than 45° to get the broad sinusoidal light curves required by the observations. Very small angles are unfavorable because they give virtually no modulation. We then derive the photon spectrum from Eq. (16) with $N_H = 1.3 \times 10^{20}$ cm^{-2}. Next, we phase average the photon spectrum. Finally, we fit this rotation phase averaged photon spectrum to a single-component blackbody to obtain T_{eff}. [6]

For models that survive the first stage, we select representative ages t_{rep} ($\gtrsim 10^5$ yr) to explore these models in more detail. Given t_{rep}, we obtain the on/off-pulse spectra and phase-averaged photon spectrum ($\theta = \psi = 30^\circ$), fold these spectra through the ROSAT PSPC detector response and fit the resultant count rate spectra (treated as "data") to single-component blackbodies to obtain the observed $T_{eff}^{on}(t_{rep})$, $T_{eff}^{off}(t_{rep})$, and $T_{eff}(t_{rep})$. The temperatures obtained in this manner are typically slightly higher (by $< 5\%$) than if folding were not performed (cf. first stage). Finally, we scan θ and ψ to assess the light curve and modulation.

6. Results and discussion

The results of fitting the models in Table 3 to the data for RX J0720.4-3125 are summarized in Table 4. The models for S stars (born slowly rotating; Sect. 5.5) include: BPS1, FP1, PS1. The models for R stars (born rapidly rotating; Sect. 5.5) include BPS2, FP2–FP6, PS2–PS10, Q1, Q2.

6.1. Modulation

It is evident from Table 4 that with few exceptions, *none* of the models can give *both* a broad sinusoidal modulation and a semi-amplitude modulation $\mathcal{M} > 9\%$ (Sect. 2). This is a consequence of using a centered dipole surface field geometry and is consistent with earlier work (e.g., Page 1995; Tsuruta & Qin 1995; Shibanov et al. 1995; see also Wang & Halpern 1997). However, several factors which are not included here could increase the modulation by as much as an order of magnitude. Atmospheric effects such as limb darkening (e.g., Zavlin et al. 1996; Rajagopal & Romani 1996; Rajagopal et al. 1997) and the anisotropic radiative transfer through magnetized atmospheres (e.g., Pavlov et al. 1994; Shibanov et al. 1995) would increase the modulation. Inclusion of more complicated field geometries can also increase the modulation. For example, using a dipole plus quadrupolar surface field geometry, Page & Sarmiento (1996) find that they can boost the *maximum* semi-amplitude modulation for a star with an FP-like EOS to around 10% and that for a BPS-like EOS to just under 5%. [7]

[6] In their modeling of RX J0720.4-3125, HH98 calculate a "flux-weighted mean temperature" over the stellar surface and compares this with the observed T_{eff}. However, what is observed is not the flux-weighted mean temperature, but rather the temperature associated with the rotation phase averaged spectrum which we calculate here.

[7] Modulations as high as 30% (14%) can be obtained for an *orthogonal* rotator using an FP-like (BPS-like) EOS, but then the light curve has two peaks, contrary to the observations of RX J0720.4-3125.

Table 3. Models[a]

Model	EOS	Mass $M_\odot$	age[b] (yr)	$\dot{P}$ (s s^{-1})	K (s)	$\bar{\omega}$ (rad s^{-1})	B (G)	cooling
BPS1	BPS	1.4	–	–	–	0	10^{12}	standard
BPS2	BPS	1.4	–	–	–	0	10^{14}	standard
FP1	FP	1.4	–	–	–	0	10^{12}	standard
FP2	FP	1.4	–	–	–	0	10^{14}	standard
FP3	FP	1.4	1.66×10^5	8.0×10^{-13}	1.70×10^{-13}	100	10^{14}	standard
FP4	FP	1.4	4.98×10^5	2.67×10^{-13}	5.67×10^{-14}	100	10^{14}	standard
FP5	FP	1.0	–	–	–	0	10^{14}	standard
FP6	FP	1.97	–	–	–	0	10^{14}	standard
PS1	PS	1.4	–	–	–	0	10^{12}	standard
PS2	PS	1.4	–	–	–	0	10^{14}	standard
PS3	PS	1.4	1.66×10^5	8.0×10^{-13}	1.70×10^{-13}	100	10^{14}	standard
PS4	PS	1.4	4.98×10^5	2.67×10^{-13}	5.67×10^{-14}	100	10^{14}	standard
PS5	PS	1.4	1.66×10^5	8.0×10^{-13}	1.70×10^{-13}	10	10^{14}	standard
PS6	PS	1.4	4.98×10^5	2.67×10^{-13}	5.67×10^{-14}	10	10^{14}	standard
PS7	PS	1.0	–	–	–	0	10^{14}	standard
PS8	PS	1.96	–	–	–	0	10^{14}	standard
PS9	PS	1.96	1.66×10^5	8.0×10^{-13}	1.70×10^{-13}	10	10^{14}	standard
PS10	PS	1.96	4.98×10^5	2.67×10^{-13}	5.67×10^{-14}	10	10^{14}	standard
Q1	BPS	1.4	1.66×10^5	8.0×10^{-13}	1.70×10^{-13}	100	10^{14}	quark
Q2	BPS	1.4	1.66×10^5	8.0×10^{-13}	1.70×10^{-13}	10	10^{14}	quark

[a] Braking index $n = 3$.
[b] Listed ages correspond to minimum age t_0 (Eqs. (4), (2)) and $3 \times t_0$.

Table 4. Results of Model Fits to RX J0720.4-3125[a]

Model	$T_{eff} = 79 \pm 4$ eV?[b]	Modulation (%)[c]	Model	$T_{eff} = 79 \pm 4$ eV?[b]	Modulation (%)[c]
BPS1	marginal	0.4	PS3	yes[e]	6.6[d]
BPS2	marginal	0.4	PS4	marginal	7.3
FP1	yes	1.9	PS5	no	7.8
FP2	marginal	2.0	PS6	no	8.9
FP3	yes	1.9	PS7	no	28.1
FP4	no	2.3	PS8	no	1.2
FP5	no	14.7	PS9	marginal	1.2
FP6	no	1.8	PS10	no	1.3
PS1	no	7.7	Q1	no	0.3
PS2	no	16[d]	Q2	no	0.25

[a] All models satisfy $T_{eff}^{on} = T_{eff}^{off}$. See Sect. 6.3 for details.
[b] For S stars (BPS1, FP1, PS1), this must be satisfied at $t_{age} \gtrsim 10^5$ yr. For R stars without heating (BPS2, FP2, FP5, FP6, PS2, PS7, PS8), this must be satisfied at $t_{age} \gtrsim t_0$ (Eq. (4)). For R stars with heating (FP3, FP4, PS3–PS6, PS9, PS10, Q1, Q2), this must be satisfied at the appropriate stellar spindown age (see Table 3). See Sect. 5.5.
[c] $\mathcal{M} \equiv (C_{max} - C_{min})/(C_{max} + C_{min})$ with C the count rate. The $\mathcal{M}$ are evaluated for $\theta = \psi = 30^\circ$ ($\theta + \psi < 90^\circ$ is required to avoid a double-peaked light curve). For the models with heating, $\mathcal{M}$ is evaluated at the appropriate stellar spindown age (see Table 3). For the models without heating, $\mathcal{M}$ is evaluated at $t_0 = 1.7 \times 10^5$ yr (Eq. (4)).
[d] $T_\perp > T_\parallel$; magnetic equator hotter than poles.
[e] Model overheats but can satisfy temperature constraint with lower $\bar{\omega}$. See Sect. 6.3 for details.

Models with the BPS EOS have extremely low modulations ($\mathcal{M} < 0.5\%$). The reason is primarily the small radii of these stars (Table 2) and consequent severe gravitational light bending. As indicated above, invoking complicated field geometries is unlikely to remedy this. It is not clear whether atmospheric effects can increase the modulation to the required level. Thus, while more accurate maximum modulations attainable by stars with a BPS-like EOS must await more detailed calculations, we regard the very small modulations obtained in our models as arguing against a soft EOS.

6.2. S stars

Fig. 3 shows the cooling curves for the S stars for the three different EOSs (BPS1, FP1, PS1 in Table 3). Since we do not specify P_i or $\dot{P}$, these stars can, in principle, have any age (cf. Eq. 11). However, we argued in Sect. 3 that an age less than $\sim 10^5$ yr is unlikely. We therefore require the S stars to fall within 79 ± 4 eV at ages $\gtrsim 10^5$ yr. Model PS1 cools too fast. Stars with the PS EOS have a substantial superfluid content and significant neutrino emission from crust bremsstrahlung (Van Riper 1991); the cooling time is $t_{cool} = U/L$, where U is the stellar heat content and L is the luminosity. Superfluidity reduces the nucleonic specific heat and hence U. In a PS star, much of the luminosity during the neutrino era is from crust bremsstrahlung, which is not affected by superfluidity. As a result, there is a net reduction in t_{cool}, which brings about an earlier end to the neutrino era so that by $t_{age} \sim 10^4 - 10^5$ yr, photon cooling takes over in the PS stars compared to $\sim 10^5$ yr in the FP and BPS stars. During the photon cooling era, the primary effect of superfluidity is to reduce U and hence t_{cool}. Stars with the PS EOS therefore cool more rapidly through both the neutrino and photon eras than those with the FP or BPS EOS.

Models FP1 and BPS1 are just able to satisfy the temperature requirement at an age $\sim 10^5$ yr. We consider the BPS1 model to be unfavorable, however, because the modulation given by this model is so low ($\mathcal{M} < 0.5\%$). Because $R \propto M^{-1/3}$ (roughly), going to smaller masses reduces the light bending ($\propto M/R$) and increases $\mathcal{M}$. Low mass stars, however, cool even faster during the photon era than shown in Fig. 3 in part because they have lower heat content (cf. Figs. 6, 7).

We conclude that if RX J0720.4-3125 was born slow (cf. Spruit & Phinney 1998), its age must be $\sim 10^5$ yr and the dense matter EOS is FP-like.

6.3. R stars

The results for our simulations of R stars, those born rapidly rotating, are shown in Figs. 4 and 5. Fig. 4 shows the cooling curves for the three equations of state without internal heating (models BPS2, FP2, PS2 in Table 3).

Acceptable models must have T_{eff} between 75 and 83 eV after at least $t_0 = 1.7 \times 10^5$ yr (Eqs. (2), (4); Sect. 5.5). As with model PS1, model PS2 cools too quickly to satisfy the temperature constraint. The FP and BPS stars succeed marginally. However, as with model BPS1, we can probably rule out the BPS star because such stars give very small modulations (Table 4).

The strength of the magnetic field affects how quickly a star cools, as illustrated in Figs. 3 and 4; for example, $B = 10^{14}\,G$ stars with the FP and BPS EOS appear hotter than the corresponding $10^{12}\,G$ stars at $t_{age} \sim 10^5$ yr, while those with the PS EOS appear colder at this age. For FP and BPS stars, neutrino emission determines the internal temperature before $\sim 10^5$ yr. In the presence of a strong field ($\sim 10^{14}$ G), thermal conduction along the field is enhanced, keeping the stellar surface in relatively effective thermal contact with the hot interior; an FP or BPS star with a strong field thus appears hotter at

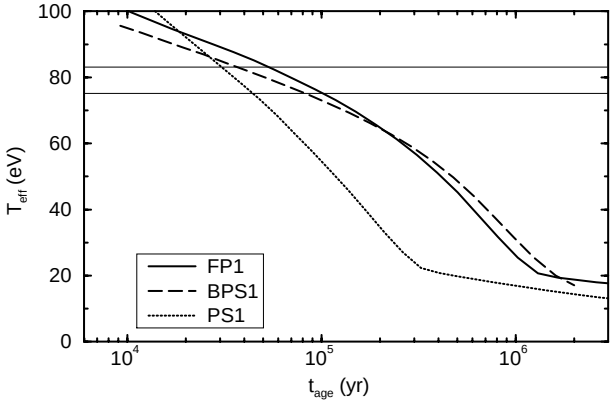

Fig. 3. The cooling curves of $1.4\,M_\odot$ S stars (Sect. 5.5) with surface dipole field strength $B = 10^{12}\,G$ for the BPS (model BPS1), FP (model FP1), and PS (model PS1) EOSs (see Table 3). These stars have essentially no internal heating because $P_i \sim P$. The horizontal lines depict the range of observed T_{eff} (79 ± 4 eV).

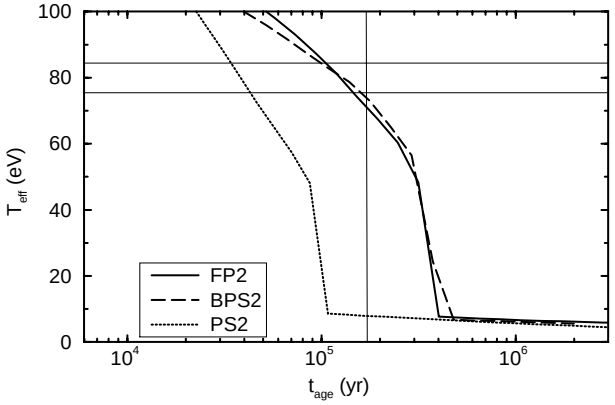

Fig. 4. The cooling curves of $1.4\,M_\odot$ R stars (Sect. 5.5) with surface dipole field strength $B = 10^{14}\,G$ for the BPS (model BPS2), FP (model FP2), and PS (model PS2) EOS (see Table 3). The internal heating is set to zero ($\bar{\omega} = 0$; Eq. (7)) in these models. The horizontal lines depict the range of observed T_{eff} (79 ± 4 eV). These stars have $P_i \ll P$ and the vertical line denotes the minimum spindown age t_0 (Eq. (4)) inferred from observations (Sect. 3). Acceptable models must fall within the horizontal lines and to the right of the vertical line (Sect. 5.5).

$\sim 10^5$ yr than a star with a weaker field (Sect. 5.1; cf. Shibanov & Yakovlev 1996). Consequently, our R-star FP and BPS models reach ~ 79 eV somwhat later than the S-star models. A PS star, however, is undergoing photon cooling before 10^5 yr; in this case, enhanced surface emission in the presence of a strong field rapidly cools the star, making it cooler at $\sim 10^5$ yr than if it had a weaker field (Sect. 5.1; cf. Shibanov & Yakovlev 1996).

HH98 were the first to model RX J0720.4-3125 as a strongly magnetized, cooling, young neutron star. They invoke a magnetar-scale field with its enhanced electron thermal conduction along the field to provide a large effective temperature at $\sim 10^5$ yr. Thus, they find that with $B = 10^{14}\,G$ and an iron envelope, the star can reach the observed T_{eff} at an age of 3.3×10^5 yr. They took the observed $T_{eff} = 69$ eV (8×10^5 K), whereas the actual best-fit blackbody temperature

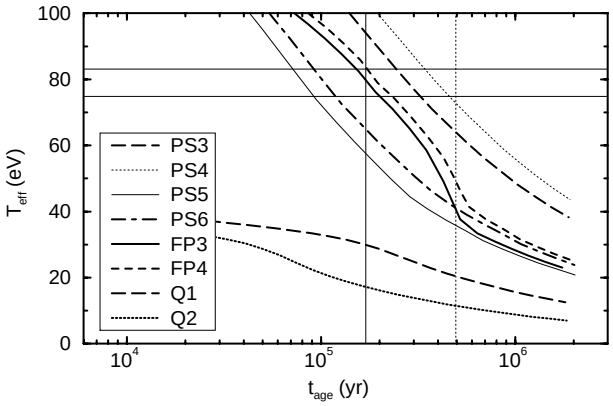

Fig. 5. The cooling curves of $1.4\,M_\odot$ R stars (Sect. 5.5) with surface dipole field strength $B = 10^{14}\,G$ including internal frictional heating (Sects. 5.2,5.3; Eq. (7)) for the PS, FP, and BPS EOS. The heating is parametrized by $\bar{\omega}$ and t_{age} (Table 3). The curves for stars with the PS EOS correspond to models PS3 ($\bar{\omega} = 100$ rad s^{-1}, $t_{age} = t_0$), PS4 ($\bar{\omega} = 100$ rad s^{-1}, $t_{age} = 3t_0$), PS5 ($\bar{\omega} = 10$ rad s^{-1}, $t_{age} = t_0$), and PS6 ($\bar{\omega} = 10$ rad s^{-1}, $t_{age} = 3t_0$). The curves for stars with the FP EOS correspond to models FP3 ($\bar{\omega} = 100$ rad s^{-1}, $t_{age} = t_0$) and FP4 ($\bar{\omega} = 100$ rad s^{-1}, $t_{age} = 3t_0$). The curves for accelerated quark cooling use the BPS EOS and correspond to models Q1 ($\bar{\omega} = 100$ rad s^{-1}, $t_{age} = t_0$) and Q2 ($\bar{\omega} = 10$ rad s^{-1}, $t_{age} = t_0$). The horizontal lines depict the range of observed T_{eff} (79 ± 4 eV). These stars have $P_i \ll P$ and the vertical solid line denotes t_0 (Eq. (4)) while the vertical dotted line denotes $3\,t_0$.

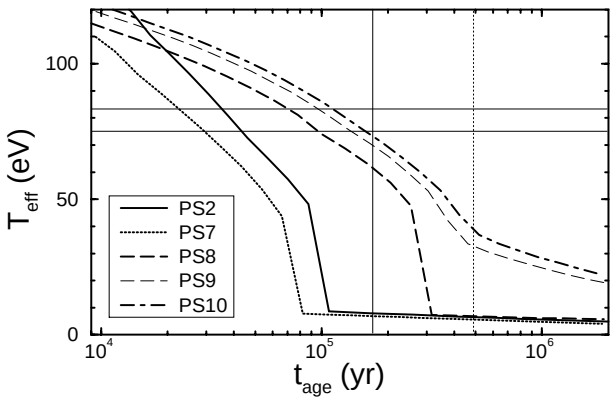

Fig. 6. The cooling curves for R stars (Sect. 5.5) with different masses. The EOS is PS and the surface dipole field strength $B = 10^{14}\,G$. The curves for $M = 1\,M_\odot$ (model PS7), $1.4\,M_\odot$ (model PS2), and $1.96\,M_\odot$ (model PS8) have no heating. The curves for $M = 1.96\,M_\odot$ have heating with ($\bar{\omega}$ [rad s^{-1}], t_{age}) = (10, t_0) (model PS9), and (10, $3\,t_0$) (model PS10). The horizontal lines depict the range of observed T_{eff} (79 ± 4 eV). These stars have $P_i \ll P$ and the vertical solid line denotes t_0 (Eq. (4)) while the vertical dotted line denotes $3\,t_0$. Acceptable models with no heating must fall within the horizontal lines and to the right of the vertical solid line (Sect. 5.5).

is $T_{eff} = 79 \pm 4$ eV (Haberl et al. 1997). Using the correct observed temperature would reduce their inferred age somewhat. It is difficult to compare our results with those of HH98 more quantitatively because of differences in the modeling such as in the treatment of neutrino cooling and superfluidity (cf. Heyl & Hernquist 1997).

Fig. 5 shows the models for ($1.4\,M_\odot$) R stars including heating (models FP3, FP4, PS3, PS4, PS5, PS6; Table 4). We consider two levels of heating: $\bar{\omega} = 100$ rad s^{-1}, which is probably the maximum that can be reasonably expected, and $\bar{\omega} = 10$ rad s^{-1}, a more realistic value. For each $\bar{\omega}$, we consider two K values that spin the star down to $P = 8.391$ sec after an age $t_0 = 1.7 \times 10^5$ yrs and $3\,t_0 = 5 \times 10^5$ yrs (corresponding to a $\dot{P} = \dot{P}_{max}/3$). The PS star with high heating (model PS3) overheats. However, since the heating rate scales as $H \propto \bar{\omega}/K^{1/2} \propto \bar{\omega}(t_S/t_0)^{1/2}$, the model can give an acceptable fit at a larger age if we reduce K (cf. Eq. (12)) and $\bar{\omega}$ while preserving the ratio $\bar{\omega}/K^{1/2}$. Thus, for example, $T_{eff} = 79$ eV would be reached at $t_S = 3 \times 10^5$ yr with $K = 9.6 \times 10^{-14}$ sec and $\bar{\omega} = 75$ rad s^{-1}. PS stars cool too rapidly if $\bar{\omega}$ is substantially less than 100 rad s^{-1}, as illustrated by model PS5. Similarly, the PS models with ages set at $3\,t_0$ (models PS4 and PS6) can marginally satisfy T_{eff} only if $\bar{\omega}$ is large (cf. PS4). [8]

[8] For a given $\bar{\omega}$, the cooling curve with the larger age (smaller K) lies above the curve with the smaller age at any given time (because $H(t) \propto \bar{\omega}/K^{1/2}$). However, this does not mean the older star is hotter, since one should compare the models when the stars have the same *period* (e.g, PS3 at t_0 is hotter than PS4 at $3\,t_0$).

For the PS stars, in order to satisfy the temperature constraint with moderate heating ($\bar{\omega} \sim 10$ rad s^{-1}), we must go to masses greater than $1.4\,M_\odot$. This is shown in Fig. 6 where we plot the cooling curves for a PS star with $B = 10^{14}\,G$ and $M = 1.96\,M_\odot$ with two heating scenarios: $\bar{\omega} = 10$ rad s^{-1} with age t_0 (model PS9), and $\bar{\omega} = 10$ rad s^{-1} with age $3\,t_0$ (model PS10). For comparison, we also show the curves with no heating for $M = 1\,M_\odot$ (model PS7), $1.4\,M_\odot$ (model PS2), and $1.96\,M_\odot$ (model PS8). High-mass stars have high heat content, and relatively low crust bremsstrahlung luminosities owing to their thin crusts, and cool the slowest. The heating run with age t_0 (model PS9) marginally satisfies the temperature constraint (cf. model PS5). As with model PS6, the heating run with age $3\,t_0$ (model PS10) still clearly fails. These results show that stars with a PS-like EOS and moderate heating can satisfy the temperature constraint only if the mass is large ($\sim 2\,M_\odot$) and the age is $\sim t_0$.

The FP star with high heating and age t_0 (model FP3) satisfies the observations, and can also do so with smaller $\bar{\omega}$ (cf. Fig. 4). However, prolonging the star's age will not work, even with high heating, as seen for model FP4. Thus, FP stars can satisfy the temperature constraint as long as their age is $\sim t_0$, regardless of the amount of heating (cf. model FP2). Increasing the stellar mass does not change our conclusions for FP stars. This is shown in Fig. 7 where we plot the cooling curves for an FP star with $H = 0$, $B = 10^{14}\,G$, and $M = 1\,M_\odot$ (model FP5), $1.4\,M_\odot$ (model FP2), and $1.97\,M_\odot$ (model FP6). Model FP6 corresponds to the maximum mass model for the FP EOS. The low-mass model (FP5) cools too quickly, owing mainly to its lower heat content. The high-mass model (FP6) appears *colder* than the $1.4\,M_\odot$ model for $t_{age} \lesssim t_0$ due mainly to larger gravitational redshift (this is a much smaller effect for a

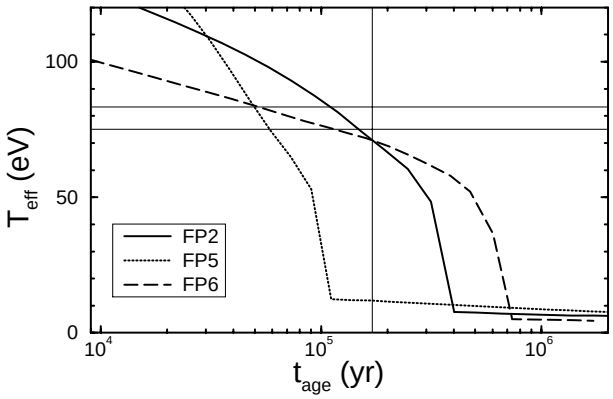

Fig. 7. The cooling curves for R stars (Sect. 5.5) with different masses. The EOS is FP and the surface dipole field strength $B = 10^{14}\,G$. The curves are for $M = 1\,M_\odot$ (model FP5), $1.4\,M_\odot$ (model FP2), and $1.97\,M_\odot$ (model FP6). The $1.97\,M_\odot$ model corresponds to the maximum mass FP star. The horizontal lines depict the range of observed T_{eff} (79 ± 4 eV). These stars have $P_i \ll P$ and the vertical line denotes t_0 (Eq. (4); Sect. 3). Acceptable models must fall within the horizontal lines and to the right of the vertical line (Sect. 5.5).

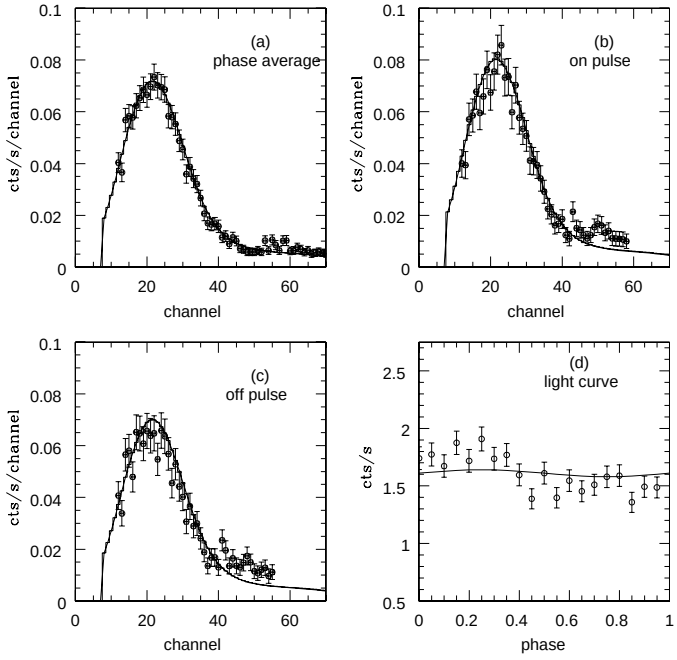

Fig. 8a–d. Comparison of model FP3 (Table 3) at age $t_0 = 1.7 \times 10^5$ yr with the data from RX J0720.4-3125. The geometrical parameters $\theta = \psi = 30^\circ$ (Sect. 5.5), and $N_H = 1.3 \times 10^{20}$ cm^{-2}. The temperatures $T_\parallel = 90$ eV and $T_\perp = 10.5$ eV are used to obtain the model curves. **a** The phase-averaged count rate spectrum. The histogram gives the model spectrum and the continuous curve gives the best single component blackbody fit ($T_{eff} = 82.5$ eV) to this spectrum. The normalization is adjusted to give 1.61 cts s^{-1} in channels 12–70 (0.1–1 keV). The ROSAT PSPC data (cf. Fig. 1 of H97) is superimposed. **b** The on-pulse count rate spectrum. The best-fit blackbody (continuous curve) to the model spectrum (histogram) has $T_{eff}(\mathrm{on}) = 82.5$ eV. The normalization is adjusted to give 1.73 cts s^{-1} in channels 12–58 (0.1–0.6 keV). The on-pulse data correspond to the spectrum between phases 0.2 and 0.7 in Fig. 3 of H97. **c** The off-pulse count rate spectrum. The best-fit blackbody (continuous curve) to the model spectrum (histogram) has $T_{eff}(\mathrm{off}) = 82.0$ eV. The normalization is adjusted to give 1.49 cts s^{-1} in channels 12–55 (0.1–0.6 keV). The off-pulse data correspond to the spectrum in phases 0–0.2 and 0.7–1.0 in Fig. 3 of H97. **d** The model light curve (semi-amplitude modulation = 1.9%) with the data superimposed. The data are folded on a period of 8.39115 sec (H97).

PS star of the same mass; cf. Fig. 6). Since a high-mass star has larger heat content, it retains heat longer and so will eventually appear hotter than the lower mass stars, gravitational redshift notwithstanding (see Fig. 7). Another factor working against a high-mass star is that the stronger light bending reduces even more the modulation $\mathcal{M}$ (Table 4). Low-mass stars give higher $\mathcal{M}$ but cool too fast.

In Fig. 5, we also show two accelerated quark cooling curves for an R star (models Q1 and Q2 in Table 3). To make the most favorable case for such stars, we include heating ($\bar{\omega} = 100, 10$ rad s^{-1} for models Q1 and Q2, respectively) and set the age to be t_0. We choose the BPS EOS because the central density of such a soft star (see Table 2) could be sufficiently high for the matter to have a significant quark content; a quark-hadron phase transition might take place at $\rho_{trans} \sim (3\text{–}6)\,\rho_{nuc} = 8 \times 10^{14}$ – 1.7×10^{15} g cm^{-3} (e.g., Prakash 1996; Jacob 1992; T. Cohen, private communication). Both models cool too fast, and the very low modulations argue further against them. We therefore conclude that the source RX J0720.4-3125, when interpreted as a cooling neutron star, cleanly rules out the presence of *any* direct URCA-type accelerated cooling mechanism. Hence, either exotic matter (or proton-rich matter) does not exist, or exotic matter (or proton-rich matter) does exist, but the corresponding direct Urca process is suppressed. The direct URCA process would be suppressed by superfluidity (see, e.g., Horvath et al. 1991; Page & Applegate 1992; Page 1994; Schaab et al. 1996; Schaab et al. 1997; Alford et al. 1998).

In Figs. 8 and 9, we show the spectra and light curves of models FP3 and PS4, and compare with the data. In panels (a)–(c), the histogram gives the model count rate spectral "data" that result from folding the photon spectrum (Sect. 5.4) through the ROSAT PSPC 256 channel detector response, and the continuous curve gives the best single-component blackbody fit to these "data". The best-fit temperatures for model FP3 are $T_{eff} = 82.5$ eV, $T_{eff}(\mathrm{on}) = 82.5$ eV, and $T_{eff}(\mathrm{off}) = 82.0$ eV. For model PS4, the best-fit temperatures are $T_{eff} = 76$ eV, $T_{eff}(\mathrm{on}) = 77$ eV, and $T_{eff}(\mathrm{off}) = 75$ eV. The values for T_{eff} are slightly higher than inferred from Fig. 5 because the temperatures here are obtained by fitting to the folded spectrum (see Sect. 5.5). Consistent with the observations, the spectra of all our models give $T_{eff}(\mathrm{on}) = T_{eff}(\mathrm{off})$ within the uncertainties in the fits (90% confidence).

7. Conclusions

In this paper we have argued that RX J0720.4-3125 is an isolated, cooling neutron star. The temperature of this source is ~ 80 eV, and the observational upper limit to the period derivative implies an age of at least $t_0 = 1.7 \times 10^5$ yr if born rapidly

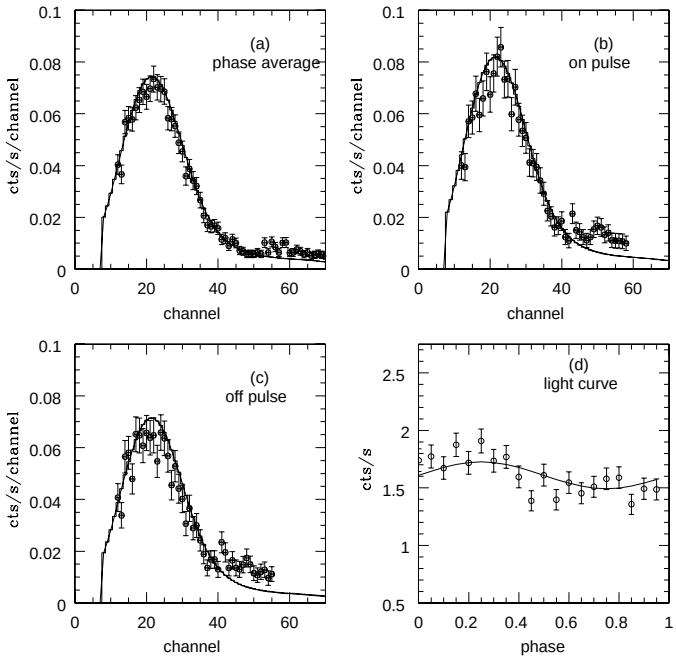

Fig. 9a–d. Comparison of model PS4 (Table 3) at age $3\,t_0 = 5\times10^5$ yr with the data from RX J0720.4-3125. The geometrical parameters $\theta = \psi = 30^\circ$ (Sect. 5.5), and $N_H = 1.3\times10^{20}\,\mathrm{cm}^{-2}$. The temperatures $T_\parallel = 83$ eV and $T_\perp = 12$ eV are used to obtain the model curves. **a** The phase-averaged count rate spectrum. Histogram gives the model spectrum and the continuous curve gives the best single component blackbody fit ($T_{eff} = 76$ eV) to this spectrum. The normalization is adjusted to give 1.61 cts s^{-1} in channels 12–70 (0.1–1 keV). The ROSAT PSPC data (cf. Fig. 1 of H97) is superimposed. **b** The on-pulse count rate spectrum. The best-fit blackbody (continuous curve) to the model spectrum (histogram) has $T_{eff}(\mathrm{on}) = 77$ eV. The normalization is adjusted to give 1.73 cts s^{-1} in channels 12–58 (0.1–0.6 keV). The on-pulse data correspond to the spectrum between phases 0.2 and 0.7 in Fig. 3 of H97. **c** The off-pulse count rate spectrum. The best-fit blackbody (continuous curve) to the model spectrum (histogram) has $T_{eff}(\mathrm{off}) = 75$ eV. The normalization is adjusted to give 1.49 cts s^{-1} in channels 12–55 (0.1–0.6 keV). The off-pulse data correspond to the spectrum in phases 0–0.2 and 0.7–1.0 in Fig. 3 of H97. **d** The model light curve (semi-amplitude modulation = 7.3%) with the data superimposed. The data are folded on a period of 8.39115 sec (H97).

rotating. The absence of a visible supernova remnant independently suggests an age of $\gtrsim 10^5$ yr. Modulation of the X-ray light curve with a semi-amplitude of $\sim 10\%$ suggests that the temperature varies over the stellar surface. We have explored the implications for the dense matter equation of state, the mode of energy loss (modified URCA vs. direct URCA), and the rate of internal heating due to superfluid friction.

If RX J0720.4-3125 was born rapidly rotating, a large average spin-down rate is required to give the observed period of 8.391 s in $\sim 10^5$ yr and the magnetic field must be of magnetar scale ($\sim 10^{14}$ G). The rapid spin-down could drive significant heating from superfluid friction. If born slowly rotating, i.e., with a period close to the present one, a small average spin-down rate is required, and the field is of modest strength ($\lesssim 10^{13}$ G). In this case frictional heating is negligible. Anisotropic heat transport in the presence of the magnetic field produces variations in the temperature over the stellar surface, which, coupled with rotation, produce a modulation of the source's light curve. The strength of the field also affects the cooling rate; for example, enhancement of the heat transport along field lines causes a star with a strong field and a soft or moderately stiff equation of state to be hotter at an age of $\sim 10^5$ yr than one with a weaker field (Figs. 3, 4).

In comparing our simulations with the data, we require that $T_{eff} = 79\pm4$ eV for $t_{age} \gtrsim 10^5$ yr (Sect. 5.5). We also consider the magnitude of the modulation for a given model in assessing its viability. Our main conclusions are:

(i) A moderately stiff EOS (FP) is consistent with RX J0720.4-3125's temperature if its age is $\sim 10^5$ yr (Figs. 3 and 4). A $1.4\,M_\odot$ star gives a modulation that is smaller than that observed by a factor of ~ 5. However, the modulation could be increased by atmospheric effects or by using more complex field geometries. Frictional heating has only a small effect at $\sim 10^5$ yr for a moderately stiff EOS.
(ii) A stiff EOS (PS) is consistent with RX J0720.4-3125's temperature if the birth period is short, the rate of heat generation from superfluid friction is significant, and the age is in the range $\sim t_0$–$3\,t_0$. An age of $3\,t_0$ requires a very high heating rate corresponding to differential rotation between the crust and inner crust superfluid of $\bar\omega \gg 10$ rad s^{-1} (Eq. (7); Figs. 4, 5). More moderate heating ($\bar\omega \sim 10$ rad s^{-1}) is adequate if the star is massive ($\sim 2\,M_\odot$), but only if the star's age is $\sim t_0$ (Fig. 6). For $1.4\,M_\odot$, the modulation is $\sim$ 7–9%, close to the observed value.
(iii) A soft EOS (BPS) is consistent with RX J0720.4-3125's temperature if its age is $\sim 10^5$ yr (Figs. 3, 4). However, this possibility is unfavored because a soft EOS gives an extremely low modulation ($\mathcal{M} < 0.5\%$; Table 5) compared to the observed $\sim 10\%$. A star with a soft EOS has a relatively low superfluid content, and frictional heating plays a negligible role at $\sim 10^5$ yr.
(iv) Low mass stars ($M \sim 1\,M_\odot$) cool too quickly and are ruled out (Figs. 6, 7).
(v) Accelerated cooling from a direct URCA process involving exotic particles or nucleons (with a proton fraction $\gtrsim 11\%$) is cleanly ruled out by RX J0720.4-3125. Hence, either exotic matter (or proton-rich matter) does not exist, or exotic matter (or proton-rich matter) does exist, but the corresponding direct Urca process is suppressed. Direct URCA reactions would be suppressed by superfluidity.

In summary, we conclude that standard cooling with a stiff or moderately stiff EOS is consistent with the observations of RX J0720.4-3125 provided the star's age is $\lesssim 3\,t_0 = 5\times10^5$ yr. This conclusion is consistent with recent RXTE observations of high amplitude ($\sim 75\%$) coherent oscillations in X-ray bursts from 4U1636-54 (Strohmayer et al. 1998) and with observations of kHz QPOs seen in low mass X-ray binaries (Kluzniak 1997; Zhang et al. 1998); both sets of observations suggest that the EOS is stiff. Theoretical studies of matter above nuclear density also indicate that the EOS is relativity stiff (see, e.g., Wiringa et al. 1988).

A measurement of $\dot{P}$ would provide a crucial test of our conclusions. For example, a measured $\dot{P} \ll 10^{-13}\,\mathrm{s\,s^{-1}}$, corresponding to a spindown age $t_S \gg 3\,t_0 = 5 \times 10^5\,\mathrm{yr}$ (cf. Eq. (4)), would rule out standard cooling, with or without internal friction, of a star born rapidly rotating. To keep the star hot ($\sim 80\,\mathrm{eV}$) long after $3\,t_0$ would require an enormous heat source. Kulkarni & van Kerkwijk (1998) have suggested decay of a magnetar field (Thompson & Duncan 1996) as such a heat source. The possibility of a long birth period and an age of $\sim 10^5$ yr would not be ruled out by the measurement of a small spin-down rate.

An important assumption in our analysis is that the true effective temperature is close to the blackbody temperature. This approximation is expected to hold for an iron atmosphere (e.g., Zavlin et al. 1996; Rajagopal et al. 1997). However, we cannot rule out the possibility of a strongly magnetized hydrogen-rich atmosphere (see footnote 3). For such an atmosphere, T_{eff} could be lower than the blackbody temperature by up to a factor ~ 2 (e.g., Shibanov et al. 1992; Rajagopal et al. 1997). An analysis that employs a magnetized H atmosphere (see, e.g., Shibanov et al. 1995) would help to further assess the detailed nature of RX J0720.4-3125.

In our treatment of neutrino emission we have ignored enhancement of the emissivity by medium effects (Voskresensky & Senatorov 1986) and the contribution of superfluid pair breaking and formation processes (Voskresensky & Senatorov 1987). Schaab et al. (1997; see also Page 1997) have shown that these effects could be important. Medium effects are difficult to estimate, but could increase the emissivity by up to 2–3 orders of magnitude. Superfluid pair breaking and formation processes could also dramatically enhance the modified URCA rate, giving a surface temperature at 10^5 yr a factor of ~ 3 lower, though this result is quite sensitive to the superfluid transition temperature for protons and/or neutrons. Inclusion of these processes, which act to lower the temperature at a given age, would lower the acceptable lower limit of RXJ0720.4-3125's age that is consistent with standard cooling models without heating. Our conclusion regarding models with heating heating would be unaltered, as the large heating rates we have considered largely control the star's thermal evolution after $\sim 10^5$ yr.

Acknowledgements. We thank J. Heyl, J. Keohane, K. Kuntz, A. Leroux, T. Strohmayer, P. Teuben, S. Tsuruta, and M. Wolfire for helpful discussions. JCLW acknowledges support of NASA Astrophysics Theory Program grant NAG5-3836 and a Graduate Research Board Award from the University of Maryland. BL acknowledges support of NASA EPSCoR grant #291748. JM acknowledges support of the DGICYT of the Spanish government through grant #PB94-0973. JCLW thanks the Physics Department at Montana State University in Bozeman, where part of this work was completed, for their hospitality. JM acknowledges the hospitality of the Institute of Geophysics and Planetary Physics at the Los Alamos National Laboratory. This research used data from the HEASARC at NASA's Goddard Space Flight Center.

References

Abney M., Epstein R. I., Olinto A., 1996, ApJ 466, L91
Alford M., Rajagopal K., Wilczek F., 1998, Phys. Lett. B 422, 247
Alpar M.A., Langer S.A., Sauls J.A., 1984, ApJ 282, 533
Alpar M.A., Cheng K.S. Pines D., 1989, ApJ 346, 823
Anderson P.W., Itoh N., 1975, Nat 256, 25
Baym G., Pethick C.J., Sutherland P., 1971, ApJ 170, 299
Becker W., Trümper J., 1997, A&A 326, 682
Bhattacharya D., Wijers R.A.M.J., Hartman J.W., Verbunt F., 1992, A&A 254, 198
Bignami G.F., Caraveo P.A., 1996, ARA&A 34, 331
Boynton P.E., 1981, In: Wielebinski R., Sieber W. (eds.) IAU Symposium 95, Pulsars. Reidel, Dordrecht, p. 279
Boynton P.E., Deeter J.E., Lamb F.K., et al., 1984, ApJ 283, L53
Brown G.E., Kubordera K., Page D., Pizzochero P., 1988, Phys. Rev. D. 37, 2042
Chanmugam G., 1992, ARA&A 30, 143
Chao N.-C., Clark J.W., Yang C.-H., 1972, Nucl. Phys. A 179, 320
Cheng K.S., Chau W.Y., Zhang J.L., Chau H.F., 1992, ApJ 396, 135
Chevalier R.A., Emmering R.T., 1986, ApJ 304, 140
Cox D.P., Anderson P.R., 1982, ApJ 253, 268
Deeter J.E., 1981, Ph.D. Thesis, University of Washington
Duncan R.C., Thompson C., 1992, ApJ 392, L9
Edgar R.J., 1986, ApJ 308, 389
Emmering R.T., Chevalier R.A., 1989, ApJ 345, 931
Epstein R.I., Baym G., 1988, ApJ 328, 680
Finley J.P., Ögelman H., Kiziloglu U., 1992, ApJ 394, L21
Friedman B., Pandharipande V.R., 1981, Nucl. Phys. A 361, 502
Friman B.L., Maxwell O.V., 1979, ApJ 232, 541
Ginzburg V.L., Ozernoy L.M., 1964, Zh. Eksper. Teor. Fiz. 47, 1030
Glendenning N.K., 1985, ApJ 293, 470
Goldreich P., Reisenegger A., 1992, ApJ 395, 250
Green D.A., 1996, A Catalogue of Galactic Supernova Remnants (1996 August version). Mullard Radio Astronomy Observatory, Cambridge, United Kingdom
Greenstein G., Hartke G.J., 1983, ApJ 271, 283
Greiveldinger C., Camerini U., Fry W., et al., 1996, ApJ 465, L35
Haberl F., Pietsch W., Motch C., Buckley D.A.H., 1996, IAUC No. 6445
Haberl F., Motch C., Buckley D.A.H., Zickgraf F.-J., Pietsch W., 1997, A&A 326, 662
Halpern J.P., Ruderman M., 1993, ApJ 415, 286
Hernquist L., 1985, MNRAS 213, 313
Heyl J.S., Hernquist L., 1997, ApJ 491, L95
Heyl J.S., Hernquist L., 1998, MNRAS 291, L69 (HH98)
Heyl J.S., Kulkarni S.R., 1998, ApJ 506, L61
Horvath J.E., Benvenuto O.G., Vucetich H., 1991, Phys. Rev. D 44, 3797
Itoh N., Kohyama J., Matsumoto N., Seki M., 1984, ApJ 285, 304
Iwamoto N., 1980, Phys. Rev. Lett. 44, 1637
Jacob M., 1992, The Quark Structure of Matter. World Scientific, Singapore, p. 362
Joss P.C., Rappaport S.A., 1984, ARA&A 22, 537
Kluzniak W., 1998, ApJ 509, L37
Konenkov D.Yu., Popov S.B., 1997, Astronomy Letters 23, 498
Kulkarni S.R., Anderson S.B., 1996, In: Hut P., Makino J. (eds.) IAU Symp. 174, Dynamical Evolution of Star Clusters. Kluwer, Dordrecht, p. 181
Kulkarni S.R., van Kerkwijk M.H., 1998, ApJ 507, L49
Lamb D.Q., 1992, In: Tanaka Y., Koyama K. (eds.) Frontiers of X-Ray Astronomy. Universal Academy Press, Tokyo, p. 33
Lattimer J.M, Pethick C.J., Prakash M., Haensel P., 1991, Phys. Rev. Lett. 66, 2701
Page D., Applegate J.H., 1992, ApJ 394, L17

Lyne A.G., Manchester R.N., 1988, MNRAS 234, 477
Maxwell O.V., 1979, ApJ 231, 201
McCray R.A., 1987, In: Dalgarno A., Layzer D. (eds.) Spectroscopy of Astrophysical Plasmas. Cambridge University Press, Cambridge, p. 255
Motch C., Haberl F., 1998, A&A 333, L59
Morrison R., McCammon D., 1983, ApJ 270, 119
Nagase F., 1989, PASJ 41, 1
Narayan R., Vivekanand M., 1983, A&A 122, 45
Narayan R., Ostriker J.P., 1990, ApJ 352, 222
Ögelman H.B., 1994, In: Kiziloglu Ü., van Paradijs J. (eds.) Lives of the Neutron Stars. Kluwer, Dordrecht, p. 101
Ögelman H., Finley J.P., 1993, ApJ 413, L31
Ögelman H., Finley J.P., Zimmermann H.U., 1993, Nat 361, 136
Page D., 1994, ApJ 428, 250
Page D., 1995, ApJ 442, 273
Page D., 1997, astro-ph/9706259
Page D., Sarmiento A., 1996, ApJ 473, 1067
Pandharipande V.R., 1971, Nucl. Phys. A 178, 123
Pandharipande V.R., Smith R.A., 1975, Nucl. Phys. A 237, 507
Pavlov G.G., Shibanov Yu.A., Ventura J., Zavlin V.E., 1994, A&A 289, 837
Pavlov G.G., Stringfellow G.S., Cordova F.A., 1996a, ApJ 467, 370
Pavlov G.G., Zavlin V.E., Trümper J., Neuhäuser R., 1996b, ApJ 472, L33
Prakash M., 1996, In: Ansari A., Satpathy L. (eds.) Nuclear Equation of State. World Scientific, Singapore, p. 229
Rajagopal M., Romani R.W., 1996, ApJ 461, 327
Rajagopal M., Romani R.W., Miller M.C., 1997, ApJ 479, 347
Reisenegger A., 1995, ApJ 442, 749
Schaab C., Hermann B., Weber F., Weigel M.K., 1997, ApJ 480, 111
Schaab C., Weigel M.K., 1998, A&A 336, L13
Schaab C., Weber F., Weigel M.K., Glendenning N.K., 1996, Nucl. Phys. A 605, 531
Schaab C., Voskresensky D., Sedrakian A.D., Weber F., Weigel M.K., 1997, 321, 591
Schaaf M.E., 1990, A&A 227, 61
Shapiro S.L., Teukolsky S.A., 1983, Black Holes, White Dwarfs, and Neutron Stars: The Physics of Compact Objects. Wiley, New York
Shibanov Yu.A., Yakovlev D.G., 1996, A&A 309, 171
Shibanov Yu.A., Zavlin V.E., Pavlov G.G., Ventura J., 1992, A&A 266, 313
Shibanov Yu.A., Pavlov G.G., Zavlin V.E., Qin L., Tsuruta S., 1995, In: Böringer H., Morfill G.E., Trümper J.E. (eds.) Proc. 17th Texas Symposium on Relativistic Astrophysics and Cosmology. Ann. NY Acad. Sci., New York, p. 291
Shibazaki N., Lamb F.K., 1989, ApJ 346, 808
Spruit H., Phinney E.S., 1998, Nat 393, L139
Stocke J.T., Morris S.L., Gioia I.N., et al., 1991, ApJS 76, 813
Stocke J.T., Wang Q.D., Perlman E.S., Donahue M.E., Schachter J., 1995, AJ 109, 1199
Strohmayer T.E., Zhang W., Swank J.H., White N.E., Lapidus I., 1998, ApJ 498, L135
Takatsuka T., 1972, Prog. Theor. Phys. 48, 1517
Thompson C., Duncan R.C., 1996, ApJ 473, 322
Thorsett S.E., Chakrabarty D., 1999, ApJ 512, 288
Tsuruta S., 1998, Phys. Rep. 292, 1
Tsuruta S., Qin L., 1995, In: Böringer H., Morfill G.E., Trümper J.E. (eds.) Proc. 17th Texas Symposium on Relativistic Astrophysics and Cosmology. Ann. NY Acad. Sci., New York, p. 299
Umeda H., Shibazaki N., Nomoto K., Tsuruta S., 1993, ApJ 408, 186
Van Riper K.A., 1991, ApJS 75, 449
Van Riper K.A., Link B., Epstein R.I., 1995, ApJ 448, 294
Verbunt F., 1994, In: Holt S.S., Day C.S. (eds.) AIP Conf. Proc. No. 308, The Evolution of X-ray Binaries. AIP, New York, p. 351
Voskresensky D., Senatorov A., 1986, JETP 63, 885
Voskresensky D., Senatorov A., 1987, Sov. J. Nucl. Phys. 45, 411
Wakatsuki S., Hikita H., Sato N., Itoh N., 1992, ApJ 392, 628
Walter F.M., Wolk S.J., Neuhäuser R., 1996, Nat 379, 233
Walter F.M., Matthews L.D., An P., et al., poster presentation at 1997 HEAD Meeting
Wang F.Y.-H., Halpern J.P., 1997, ApJ 482, L159
Wang J.C.L., 1997, ApJ 486, L119 Erratum: ApJ 497, L55 (1998)
Wang J.C.L., Sutherland R.S., 1998, In: Holt S.S., Kallman T.R. (eds.) AIP Conf. Proc. No. 431, Accretion Processes in Astrophysics: Some Like it Hot! AIP, New York, p. 413
Welsh B.Y., Craig N., Vedder P.W., Vallerga J.V., 1994, ApJ 437, 638
Wiringa R.B., Fiks V., Fabrocini A., 1988, A. Phys. Rev. C 38, 1010
Yakovlev D.G., Levenfish K.P., 1995, A&A 297, 717
Zavlin V.E., Pavlov G.G. Shibanov Yu.A., 1996, A&A 315, 141
Zhang W., Smale A.P., Strohmayer T.E., Swank J.H., 1998, BAAS 30, 932